

Processing and Characterization of PET Composites Reinforced With Geopolymer Concrete Waste

Ana Paula dos Santos Pereira^a, Marcelo Henrique Prado da Silva^a, Édio Pereira Lima Júnior^a,

Andersan dos Santos Paula^a, Flávio James Tommasini^{a*}

^aInstituto Militar de Engenharia - IME, Departamento de Engenharia Mecânica e de Materiais, Pça. Gen. Tibúrcio, 80, Praia Vermelha, Urca, Rio de Janeiro, RJ, Brazil

Received: August 14, 2017; Accepted: September 04, 2017

In the present study, poly (ethylene terephthalate)-based composites were produced and characterized. These composites were composed by poly (ethylene terephthalate) (PET) reinforced with geopolymer concrete waste (GCW). Both untreated (U-GCW) and treated with oleic acid (OA) geopolymer concrete waste (T-GCW) were used in the production of the composites. The PET/GCW ratios used for either treated or untreated GCW bodies were 80/20 (wt%), 60/40 (wt%) and 50/50 (wt%). Chemical compositions were assessed by X-ray fluorescence spectroscopy (XRF), crystallinity by differential scanning calorimetry (DSC), thermal stability by thermogravimetry (TGA), microstructure by field emission gun scanning electron microscopy (FEG-SEM) with energy dispersive X-ray spectroscopy (EDS), and mechanical properties were assessed by compression tests. Fourier transform infrared spectroscopy (FT-IR) was used to check the efficiency of the treatment with OA, as well as the interaction between PET and GCW. The T-GCW PET composites showed better thermal, physical, and mechanical properties, for non-structural applications, when compared to U-GCW.

Keywords: PET composites, geopolymer concrete waste, poly (ethylene terephthalate), oleic acid, melt processing.

1. Introduction

The incorporation of inorganic fillers to polymer matrixes has been the subject of several studies.¹⁻⁵ Gorrasi *et al.*² prepared and characterized the physical properties of a PET-based composite reinforced by dispersed halloysite nanotubes for packaging applications. According to these authors, the behavior of the composites was similar to that observed in the literature. Kilinc *et al.*³ investigated the flame retardancy and tensile properties of PET-based composites containing phosphorus and boron-based additives, which were processed by extrusion and subsequently molded in an injection machine. These authors reported a high flame retardancy and strength improvement after the additions. However, other authors have investigated the properties derived by the addition of the Fe₂O₃, CaCO₃, TiO₂, and ZnO nanofillers⁴. Chae *et al.*⁵ studied the thermal and rheological properties of highly concentrated PET composites with ferrite nanoparticles. The results showed that ferrite nanoparticles played an important role in PET crystallization, due to heterogeneous nucleation.

Consequently, other characteristics were influenced, such as the thermal stability of the matrix by obstruction of the heat permeability and low diffusion of volatile degradation products. The tensile strength and rupture energy of hybrid poly (methyl vinyl siloxane) composites reinforced with short PET fibers and wollastonite whiskers were studied

by Fu *et al.*⁶ The authors observed an increase in strength with increasing wollastonite content, from 5 to 45 wt%. The authors expected an opposite effect, due to change on the interface properties between PET fibers and matrix, caused by the incorporation of wollastonite whiskers. However, interfacial frictional stress caused by matrix shrinkage during the curing process may have accounted for the strengthening of the composite. In another study, Scaffaro *et al.*⁷ reported the effect of nature and content of organically modified clay on the properties of PET nanocomposites. However, the filler content used were low (3, 5 and 10 wt%) for each kind of Cloisite clay (15A and 30B), when compared to the contents used in the present study. These authors indicated intercalated structure for the lowest clay content (3 wt%), while increasing filler amount induced the coalescence of clay particles, and a coarse morphology. These authors observed the trend of strong degradation of the PET during processing due the presence of organic modifier, a slight increase in crystallinity and a slight change on Young's modulus for all clay contents below 10 wt%.

The class of aluminosilicates is based on [SiO₄] and [AlO₄] tetrahedral units, that are reactive inorganic oxides in solution. Cement-derived materials, such as geopolymers, are composed by several kinds of aluminosilicates, ferroaluminates and other compounds, which can be extracted from fly ash, mud, ground granulated blast furnace slags, coal ash, rice husk ash, kaolinite, metakaolinite, palm oils and others. This utilization decreases the amount of urban solid waste^{8,9}.

*e-mail: fallmasini@ima.ufjf.br

Controlling morphology, granulometry crystallinity and chemical composition is effective in optimizing density, sulfate resistance, chloride resistance, mechanical properties, sustainability and costs^{10,11,12}.

The purpose of this study was to develop composites containing high amounts of pulverized geopolymers concrete waste, treated and untreated with oleic acid. The results highlight the potential of the composites in the substitution of conventional materials by novel composites with optimized thermal stability, thermal-acoustic insulation, density, mechanical resistance and processability.

2. Materials and Methods

The poly (ethylene terephthalate) (PET) was provided by the Instituto de Macromoléculas Professora Eloisa Mano (IMA); the geopolymer concrete waste (GCW) was supplied by Lafarge Concrete Ltda and the oleic acid (OA, 99% purity) was purchased from Sigma Aldrich.

The GCW fillers were modified by a treatment with oleic acid (OA), in which 100 g of the geopolymer concrete particles were added to 450 ml of a 0.33% (v/v) OA solution in ethanol. The OA treatment was kept under stirring during 24 hours, and the treated geopolymer materials were filtered and washed with ethanol to remove the unreacted oleic acid. After that, treated and untreated materials were dried. Consequently, the materials were referred as untreated geopolymer concrete waste (U-GCW) and treated geopolymer concrete waste (T-GCW). The modification was performed in an attempt to compatibilize organic and inorganic phases, dispersing the hybrid fillers and increasing fluidity of the melt polymer¹³.

The composite specimens were processed by hot pressing the mixed pulverized PET and T-GCW or U-GCW at 270°C, in proportions 80/20 (wt%), 60/40 (wt%) and 50/50 (wt%). Cylinder PET/U-GCW and PET/T-GCW specimens were produced for the compression tests, according to ASTM D695. Therefore, 06 groups of composites were produced and characterized.

Chemical composition triplicates of the geopolymer concrete waste were evaluated by X-ray fluorescence analysis (XRF) in a Rigaku RIX 3100 spectrometer. The amount of each oxide was determined and expressed in terms of mass percentage (wt%).

Fourier transform infrared spectroscopy (FT-IR) was performed with a Shimadzu, Model IR-21 PRESTIGE spectrometer, using a KBr disk. The spectra were taken from 400 to 4000 cm⁻¹ with 128 scans and 2 cm⁻¹ of resolution. Characteristic absorptions bands of the processed composites were registered.

Thermal degradations of the composites were assessed by means of a TA Instrument Q500 thermogravimetry (TGA) equipment. The analyses were carried out from 30 to 700°C, at 10°C/min, under nitrogen atmosphere. 10 mg

samples were analyzed. The onset, maximum degradation and end temperatures (T_{onset} , T_{max} and T_{end}) were registered and compared.

Differential Scanning Calorimetric (DSC) analyses were carried out using a TA Instruments Q1000 calorimeter. The polymer composites were heated from 30 to 300°C at 10°C/min. All composites were heated and kept at the maximum temperature during 2 min, and cooled to the minimum temperature (30°C) at 10°C/min. This first step aims to bring the composite to the as-received condition. After this, the bodies were heated up to 300°C at 10°C/min. The crystallinity grades of the composites were calculated for each material according to the methodology described elsewhere¹⁴. The overlay of the curves is shown between the temperatures at 30 and 300°C.

The morphology, dispersion of particles and interface structure of the composites were observed in a field emission gun scanning electron microscope (FEG-SEM), model FEG QUANTA 250 (FEI), with accelerate voltage of 30 kV. The samples were placed coated with a platinum layer for avoiding charging. The compositions of samples were evaluated and confirmed by energy dispersive X-ray spectroscopy (EDS) analysis.

The mechanical properties were determined in a tensile-compression test machine (EMIC DL 10000), equipped with a 100 kN compression-tension cell. The tests were performed at 25°C at a strain rate of 1.3 ± 0.3 mm/min. Cylindrical specimens were machined to the dimensions of 2.5 cm diameter and 5 cm height, required for plane strain compression tests by ASTM 695. The strain percentage of the stress-strain curves was normalized with respect to the initial sample dimensions¹⁵.

3. Results and Discussion

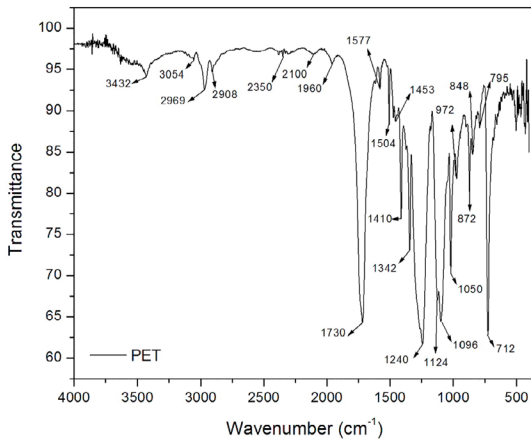
X-ray fluorescence data are presented in the Table 1. SiO₂, CaO, Al₂O₃, Fe₂O₃ and K₂O were the major components. According to the literature, these oxides are the main components of geopolymer concrete^{16,17,18}.

FT-IR analyses allowed the identification of the functional groups present on PET polymer, U-GCW and T-GCW. Figure 1 shows the corresponding infrared absorption bands of PET polymer. The identified vibrational groups are summarized on the Table 2. The bands are in agreement with Edge *et al.*¹⁹ and Silverstein and Webster²⁰.

Table 3 shows the summarized results of FT-IR analysis for the U-GCW sample, with literature references. The absorption bands of the U-GCW were detected at 3440 cm⁻¹ (O-H, stretch), 2516, 2348 and 1796 cm⁻¹ (C=O; calcite, CaCO₃), 1640 cm⁻¹ (H-O-H, bond), 1423 cm⁻¹ (C=O e OH, stretching), 1000 (Si-O; silicate, C-S-H), 874 cm⁻¹ (C=O, stretching, calcite, CaCO₃) e (aluminate phase, Al-O), 776 cm⁻¹ (Si-O-Si, symmetrical stretching), 713 cm⁻¹ (CO₃, stretching), 678 - 648 cm⁻¹ (SiO₄, stretching) e 583 - 414 cm⁻¹ (Fe-O-Fe, stretching)^{20-25,29-34}.

Table 1. Chemical composition of the U-GCW obtained by X-ray fluorescence.

Quantitative Results			
Analyte	Content (%)	Analyte	Content (%)
SiO ₂	46.708	TiO ₂	0.903
CaO	24.419	MnO	0.180
Al ₂ O ₃	14.362	SrO	0.094
K ₂ O	4.355	ZrO ₂	0.085
Fe ₂ O ₃	3.829	Rb ₂ O	0.015
SO ₃	2.768	ZnO	0.013
MgO	2.274	Y ₂ O ₃	0.005

**Figure 1.** FT-IR spectrum of the PET sample.

The efficiency of the OA treatment process in the compatibilization of the hybrid fillers is clear in Figure 2, which shows the overlay of the untreated and treated fillers.

The T-GWC samples presented the new absorption bands of the OA in the regions at 713 cm⁻¹ (C-[CH₂]_n-C, skeletal stretching vibration), 938 cm⁻¹ (O-C-OH, bending

vibration), 1285 cm⁻¹ (C-O, bending vibration), 1378 cm⁻¹ (CH₃, symmetrical deformation), 1420 (OH, bending vibration), 1468 cm⁻¹ (CH₂, bending vibration), 1736 cm⁻¹ (C=O, stretching), 2852 and 2924 cm⁻¹ (CH₂ e CH, asymmetrical and symmetrical stretching), which suggest the surface modification of the geopolymeric fillers^{19-25,29-34}. Table 4 summarizes these results.

According to Figures 3 and 4, the PET/U-GCW and PET/T-GCW composites presented the absorptions corresponding to fillers of the geopolymer concrete waste and assigned to functional groups ascribed. The spectra of the PET/U-GCW, 80/20, 60/40 and 50/50 revealed the polymeric absorption bands with lower intensities than treated composites. It suggests that the compatibilization between the surface of the treated fillers and the polymer has occurred, providing a good adhesion between matrix and filler. As expected, the increase on filler amount was compatible with decreasing intensities of the absorption bands corresponding to the PET, for all composites, while increasing intensities of the geopolymer concrete waste bands were observed.

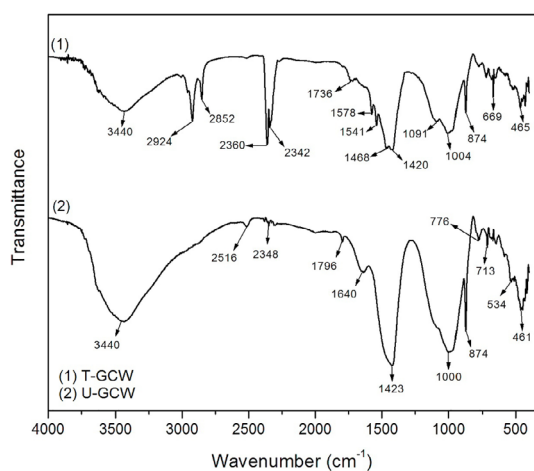
The thermal stability of the PET, neat and treated geopolymer concrete as well as hybrid composites were evaluated by thermogravimetric analysis. Figure 5 presents the data of TG/DTG corresponding to PET. The TG/DTG curves of the PET polymer showed one degradation step, with T_{onset} around at 340°C, indicating the loss of vinyl ester and acid end groups and the formation of cyclic oligomers. The DTG curve indicated T_{max} at 434°C, which represents the decomposition of cyclic oligomers and release of acetaldehydes groups and anhydrides oligomers²⁶. The values of weight loss of all materials, T_{onset}, T_{max} and T_{end} are presented in Table 5. Untreated geopolymer concrete waste and treated geopolymer concrete waste showed different behaviors (Figure 6). Initially, one peak of mass loss at 71°C and 77°C can be observed for each geopolymer material, untreated and treated, respectively. The effects can be attributed to

Table 2. Bands with assigned vibrational modes from FTIR spectrum of the PET sample.

Absorption bands (cm ⁻¹)	Bands
3432	OH group (hydroxyl) ^{19,20}
3054	Symmetrical stretch of CH ²⁰
2969 and 2908	C-H, Symmetrical stretching ²⁰
2350	Axial symmetrical deformation of CO ₂ ²⁰
1730	Stretching of C=O of carboxylic acid group ¹⁹
1577 and 1504	Vibrations aromatic skeleton with stretching C=C ¹⁹
1453, 1410 and 1342	Stretching of the C-O group deformation of the O-H group ^{19,20} and bending and wagging vibrational modes of the ethylene glycol segment ²¹
1240 and 1124	Terephthalate Group (OOC ₆ H ₄ -COO) ¹⁹
1096 and 1050	Methylene group ²¹ and vibrations of the ester C-O bond ²⁰
972, 872 and 848	Aromatic rings 1,2,4,5; Tetra replaced ^{19,20}
1960 and 795	Vibrations of adjacent two aromatic H in p-substituted compounds ^{19,20} and aromatic bands ²¹
712	Interaction of polar ester groups and benzene rings ¹⁹

Table 3. Characteristics of U-GCW FTIR spectrum.

Absorption bands (cm ⁻¹)	Bands
3447	O-H, stretch ^{20,22,34}
2516, 2348 and 1796	C=O; calcite, CaCO ₃ ²²
1640	Stretching vibration of O-H ³¹
1423	Stretching C=O ²² and O-H ²⁸
1000	Si-O; silicate, C-S-H ^{20,22,30,31}
874	C-O, calcite, CaCO ₃ ^{22,29}
796	Si-O-Si, symmetrical stretching ^{32,33}
713	CO ₃ , stretching ³²
534	Si-O-Si out of plane bending mode ³³
461	Si-O, stretching ³²

**Figure 2.** Overlay of the FT-IR spectra of T-GCW and U-GCW.

liberation of free water present into pulverized materials, as C-S-H type or N-A-S-H gels and free water liberated by reaction between the oleic acid with hydroxyl groups onto the surface of the geopolymer materials during the modification

synthesis^{13,27}. According to curves of untreated geopolymer and treated material can suggest the efficiency of the surface chemical modification with oleic acid. The effect was more evident by elucidated event with high loss weight at 447°C.

Figures 7 and 8 show the TG/DTG curves for the PET/U-GCW composites. The results show the increase on the thermal stability of the composites (80/20, 60/40 and 50/50) with increasing filler content, and the degradation onset temperature was observed at 374°C, with residue content of 66%, 51% and 44%, respectively. The first step presents the T_{max} of the PET/U-GCW in the range of 431-437°C, which corresponding to degradation of the polymer. The second step was detected at 580°C and can be attributed to thermal decomposition of the calcium hydroxide, while the third step (around to 680°C) can correspond to silica dehydroxylation, decomposition of aluminates and carbonates of the geopolymer concrete^{13,14,18}. These behaviors reveal no chemical interaction between PET and filler content on untreated composites. Figure 9 shows the TG curve of the treated hybrid composites. According to results, the obtained esterification of the hybrid fillers favored the compatibilizing with the polymer matrix, what raised the thermal stability of the PET/T-GCW composites. The T_{onset} of the treated composites (80/20, 60/40 and 50/50), were displaced to range of 380°C and the amount of residues, 63%, 59% and 40%, were related to the efficient compatibilization between the fillers and polymer with the insertion of the OA. The DTG curves of the PET/T-GCW composites show one initial degradation temperature around to 263°C that was related to ebullition of the OA and the three steps of degradation of the composite samples. DTG curves (Figure 10) of the PET/T-GCW composites presented the three steps of degradation with similar temperatures those were observed between the PET/U-GCW composites corresponding to events described.

The T_g of the polymer was detected at 78°C. The effects of the high proportions of geopolymer concrete

Table 4. Characteristics bands of the T-GCW FTIR samples obtained by FT-IR.

Absorption bands (cm ⁻¹)	Bands
3440	O-H, stretch ^{20,22,34}
2924, 2852, 1578 and 1541	Group vibrations CH ¹³ and CH ₂ ³⁴
2360 and 2342	Symmetric axial deformation of the CO ₂ ²⁰
1736	Stretching vibration of O-H ³³
1468	C=O e OH, stretching and CH ₂ Vibrational deformation ^{33,34}
1420	C=O e OH, stretching ^{22,29}
1091	Si-O-Si asymmetric stretching vibration ^{22,30,33}
1004	Si-O; silicate, C-S-H ^{20,22,31}
874	C-O, calcite, CaCO ₃ ^{22,29}
669	Si-O bending ^{22,32}
465	O-Si-O, bending vibration ^{32,33}

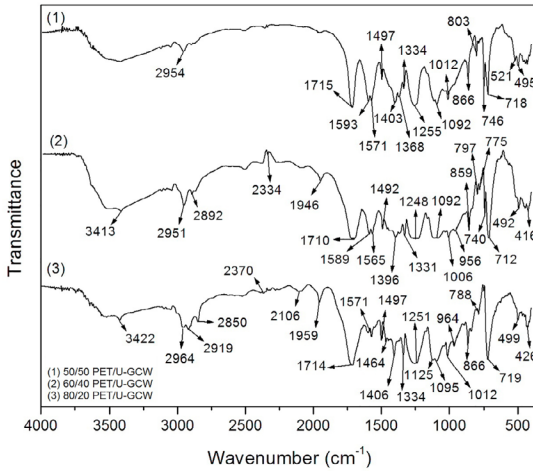


Figure 3. Overlay of the FT-IR spectra for the PET/U-GCW composites.

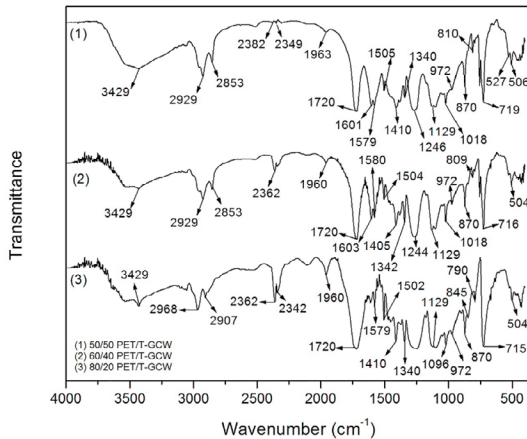


Figure 4. Overlay of the FT-IR spectra for the PET/T-GCW composites.

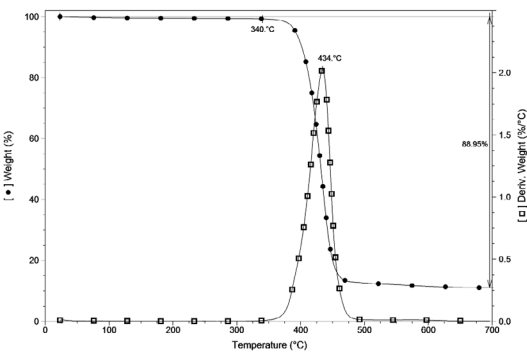


Figure 5. TG and DTG curves for the PET samples.

waste (untreated or treated) into the processed polymer matrix on melting and crystallization temperatures (T_m , T_c), and degree of crystallinity were observed and analyzed (Table 6). The T_m peaks of the all processed polymeric composites are slightly lower or higher than observed for

PET. This effect can be attributed to lower crystallinity of the polymer in the composites by high amount of fillers embedded into the polymer matrix, which made recrystallization difficult of PET chains. The influence to 80/20 composites with and without treatment was lower, what can be explained by higher polymer proportion. This led to a slight increase in T_m value. The crystallinity degree (X_c) of the PET matrix in the composites treated with oleic acid was lower than no treatment composites. Probably, the long chain of OA, anchored onto the fillers and polymer chain hampered the better crystallization^{28,29}. This result is in accordance with the better processability and dispersion of fillers observed by FEG-SEM microscopy.

FEG-SEM electron micrographs (Figures 11 and 12) show embedded fillers into the polymer matrix, observed for both composites; this finding suggests that the melt processing of the PET was efficient. However, the treated composites showed the development of a more compacted structure, what can corroborate the efficiency of the surface treatment with OA compatibilizing both the inorganic surface of fillers and organic material. The electron micrographs of the external surfaces of all molded specimens show the polymeric matrix with several kinds of fillers disperses into the polymer, thereby the molding processing of higher amount of geopolymer concrete waste into the PET polymer was effective (Figures 13 and 14). The images showed better dispersions of the GCW to all the treated composites than no treatment composites with the increase in the amount of geopolymer concrete waste. The created porosity in the composites are the results of the releasing of the gases during the melt PET processing to molding of the specimens, however can exist some influence of the releasing of free water present into the filler, as observed by thermogravimetry results. The higher porosity of the composites 60/40 and 50/50 can suggest that the covered filler interfered in the output of gas liberated by melting of the PET. The EDS spectra of the composites showed the presence of high amount of elements presented into the aluminosilicates materials and carbon. These results corroborated with XFR and FT-IR analysis, which confirmed the composition of the geopolymer concrete waste and presence of the polymer in the composites.

The specimens with higher proportions of polymer exhibited a less pulverulent, brighter and smooth surface. This is due to the polymer present in the composites migrating to the surface of the specimen, promoting the appearance of a film, this effect being similar to the core-shell (Figure 15). Results of compression tests in the composite specimens molded under the melt state containing high geopolymer concrete waste contents. Figure 16 shows the compression tests results for the PET/U-GCW and PET/T-GCW composites. The 50/50 composites presented the highest mechanical performance,

Table 5. TG/DTG properties of the specimens.

Samples	T _{onset1} (°C)	T _{max1} (°C)	T _{end1} (°C)	T _{onset2} (°C)	T _{max2} (°C)	T _{end2} (°C)	T _{onset3} (°C)	T _{max3} (°C)	T _{end3} (°C)	Residues (%)
PET	374	434	468	---	---	---	---	---	---	11
U-GCW	45	60	71	389	422	431	591	667	685	82
T-GCW	46	77	108	374	447	508	616	672	686	74
PET/U-GCW 50/50	335	431	470	526	577	614	664	684	696	56
PET/U-GCW 60/40	358	435	471	537	573	603	642	667	690	49
PET/U-GCW 80/20	350	437	482	548	583	615	---	---	---	34
PET/T-GCW 50/50	347	426	478	534	573	597	654	683	695	52
PET/T-GCW 60/40	350	434	474	533	574	600	655	680	696	40
PET/T-GCW 80/20	351	435	492	530	574	616	---	---	---	31

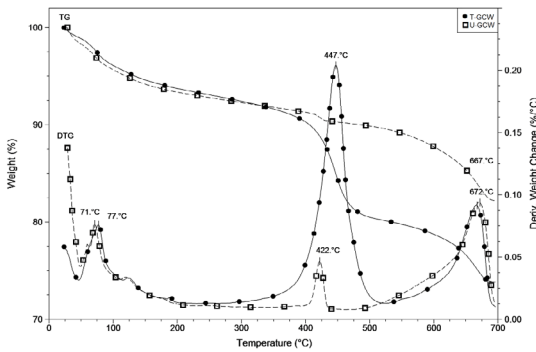


Figure 6. Overlay of the TG and DTG curves of T-GCW and GCW composites.

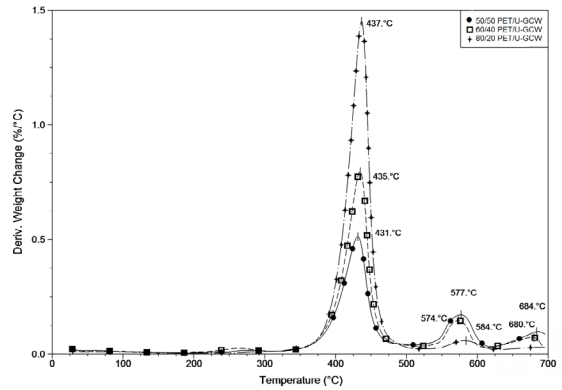


Figure 8. Overlay of the DTG curves of PET/U-GCW composites.

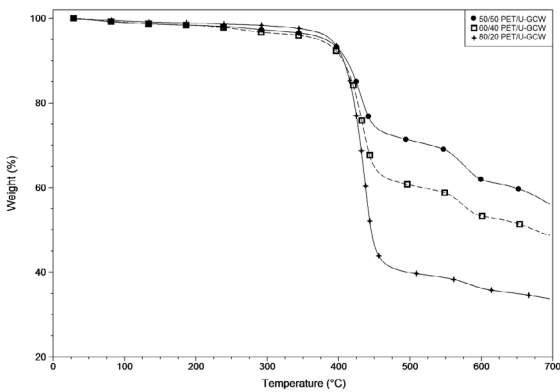


Figure 7. Overlay of the TG curves of PET/U-GCW composites.

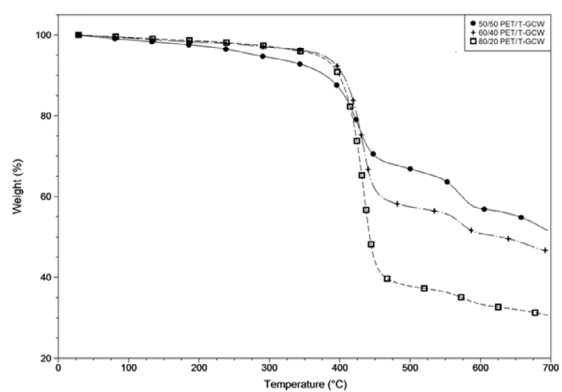


Figure 9. Overlay of the TG curves of PET/T-GCW composites.

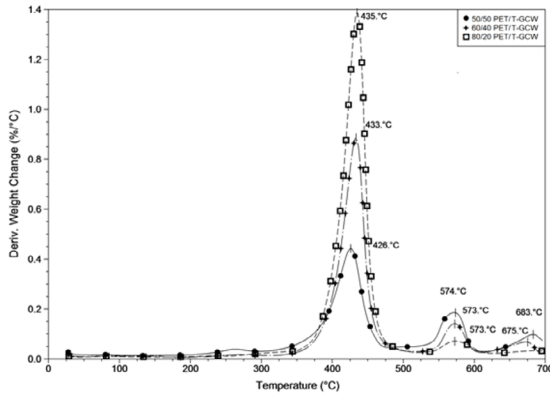


Figure 10. Overlay of the DTG curves of PET/T-GCW composites.

and this finding is probably due to the low PET content, contributing to a rigid of the composite specimens.

After the compression test, a high concentration of pores was observed for all samples, which corroborated with the FEG-SEM analyses. The porous structure of hybrid composites was assigned as results of the release of a high amount of CO_2 , in which a low amount was retained into the PET matrix. Fragility places of the composites were associated to the voids created and contributed to the rupture of all samples. Table 7 shows the compression resistance of the composites. The results presented the better compression properties for treated hybrid composites, what can corroborate with the efficiency

Table 6. Calorimetric properties of the specimens.

Samples	T_m (°C)	T_c (°C)	ΔH_m (J/g)	ΔH_c (J/g)	X_c (%)
PET	246.25	199.03	44.21	45.20	31.58
50/50 PET/U-GCW	239.04	162.72	1.72	0.80	2.46
60/40 PET/ U-GCW	244.33	171.91	9.50	6.25	11.31
80/20 PET/ U-GCW	252.08	200.54	28.87	25.67	25.78
50/50 PET/T-GCW	223.30	107.30	0.28	0.34	0.40
60/40 PET/ T-GCW	229.15	163.09	5.82	5.78	6.93
80/20 PET/ T-GCW	246.44	204.71	26.43	23.56	23.60

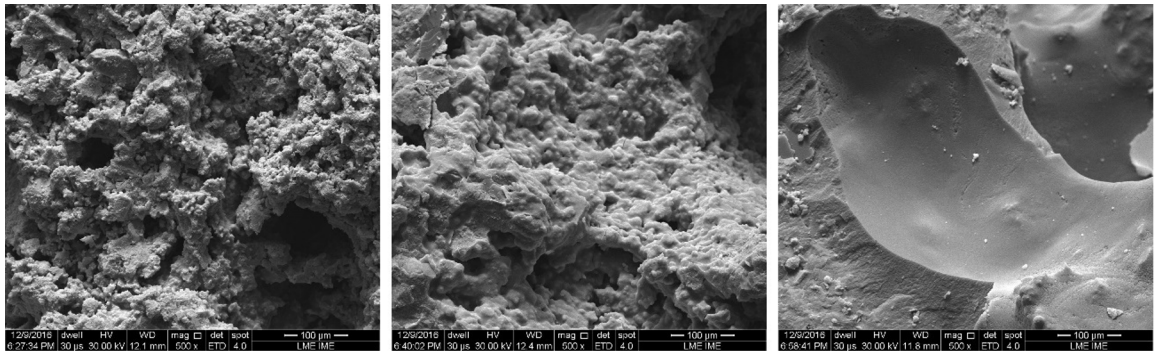


Figure 11. SEM electron micrographs of fracture of the PET/U-GCW composites: (a) 50/50 (b) 60/40 and (c) 80/20.

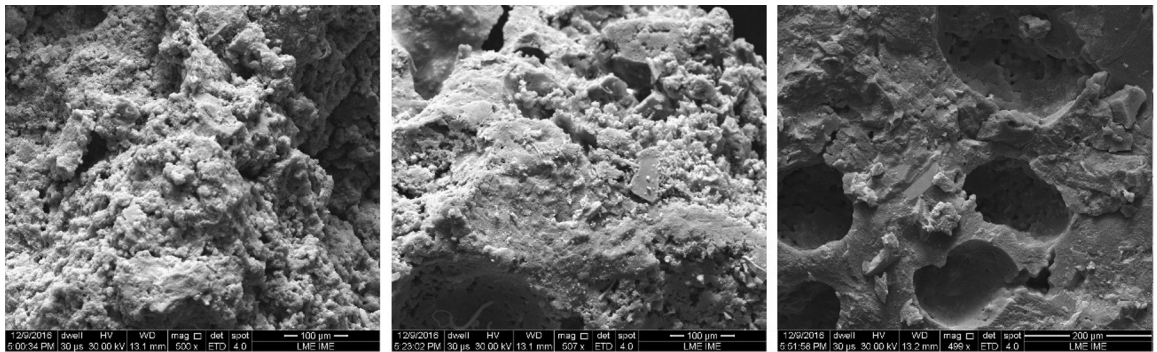


Figure 12. SEM electron micrographs of fracture of the PET/T-GCW composites: (a) 50/50 (b) 60/40 and (c) 80/20.

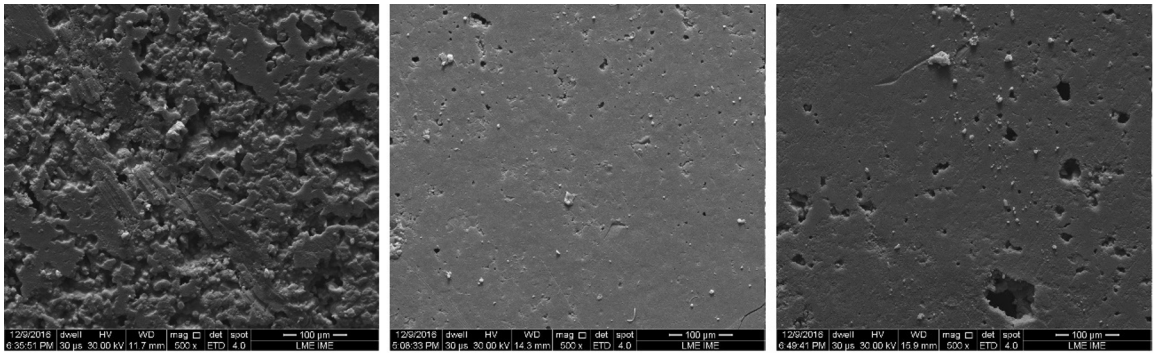


Figure 13. SEM electron micrographs of the surfaces of the PET/U-GCW composites: (a) 50/50 (b) 60/40 and (c) 80/20.

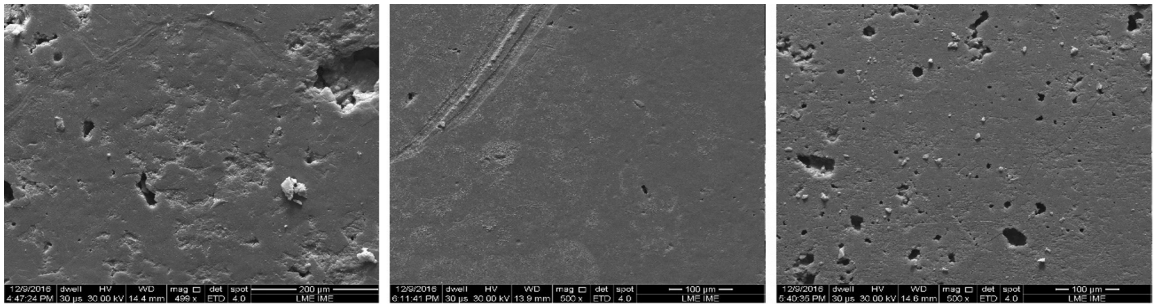


Figure 14. SEM electron micrographs of the surfaces surface of the PET/T-GCW composites: (a) 50/50 (b) 60/40 and (c) 80/20.

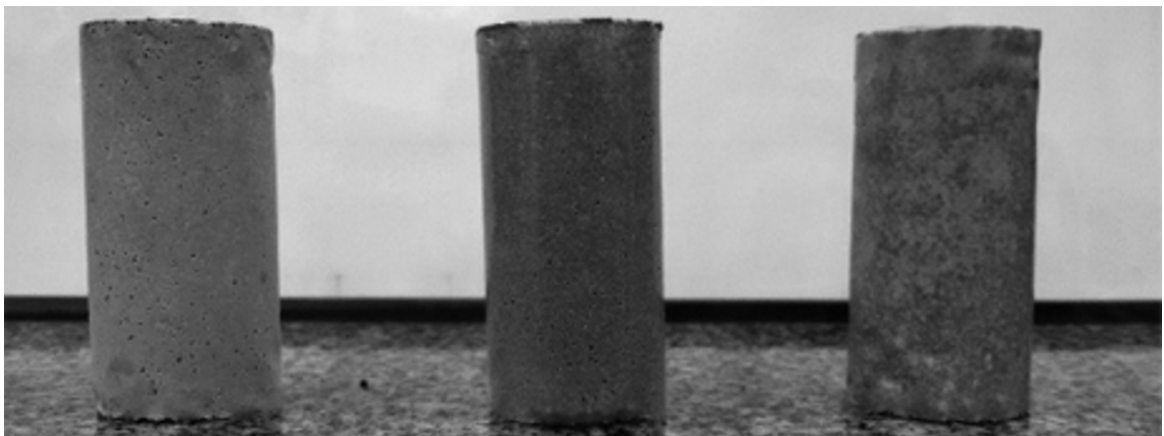


Figure 15. Specimens of the composites 50/50, 60/40 and 80/20 PET/T-GCW (from left to right).

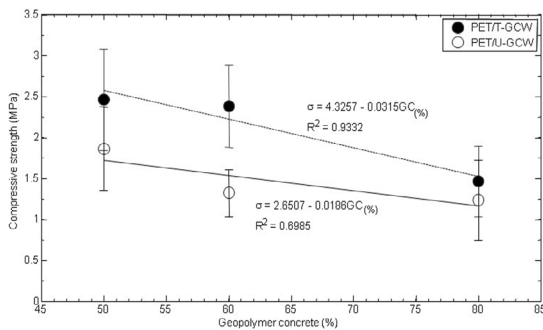


Figure 16. Graphic of compression test with standard deviation of the PET/U-GCW and PET/T-GCW.

Table 7. Values of the compression test of the PET/U-GCW and PET/T-GCW composite specimens.

Samples	Compressive strength (MPa)
50/50 PET/ U-GCW	1.86 ± 0.51
60/40 PET/ U-GCW	1.32 ± 0.29
80/20 PET/ U-GCW	1.23 ± 0.49
50/50 PET/ T-GCW	2.46 ± 0.62
60/40 PET/ T-GCW	2.38 ± 0.50
80/20 PET/ T-GCW	1.46 ± 0.43

onto surface compatibilization of the hybrid fillers and polymeric chains.

4. Conclusion

X-ray fluorescence and FT-IR analyses confirmed the geopolymer composition of the concrete waste, while the increase of the thermal stability of the polymer with higher amount of fillers in the composites was attested by thermogravimetric analysis (TGA).

DSC analysis permitted to verify the lower crystallization degree for treated geopolymer concrete waste composites than untreated geopolymer concrete waste composites and poly (ethylene terephthalate), which corroborate with the effect of the good dispersion of treated fillers and the difficulty to recrystallization of the polymer due the long chain of the oleic acid between polymer and filler surface.

The results of the study showed the melt processability and moldability of all composites by heat pressing.

The compatibilization between the geopolymer concrete waste and organic matrix was efficient and reflected in better compression resistance to the treated composites.

The good adhesion between filler and polymer was observed in the treated composites by FEG-SEM, what can be attributed to presence of oleic acid arrested onto the geopolymer concrete waste surfaces. Mechanical tests allowed to verify the good performance between all composites, however showed that the effect of the compatibilizing improved the better results between the composites.

5. Acknowledgments

The authors would like to acknowledge Conselho Nacional de Desenvolvimento Científico e Tecnológico (CNPq) and Coordenação de Aperfeiçoamento de Pessoal de Nível Superior (CAPES) for funding this research, and Instituto Militar de Engenharia (IME) and Instituto de Macromoléculas Professora Eloisa Mano (IMA) for the technical support for this work.

6. References

- Ramos FJHTV, Mendes LC. Recycled high-density polyethylene/gypsum composites: evaluation of the microscopic, thermal, flammability, and mechanical properties. *Green Chemistry Letters and Reviews*. 2014;7(2):199-208.
- Gorrasi G, D'Ambrosio S, Patimo G, Pantani R. Hybrid clay-carbon nanotube/PET composites: Preparation, processing, and analysis of physical properties. *Journal of Applied Polymer Science*. 2014;131(13):40441.
- Kilinc M, Cakal GO, Bayram G, Eroglu I, Özkaz S. Flame retardancy and mechanical properties of pet-based composites containing phosphorus and boron-based additives. *Journal of Applied Polymer Science*. 2015;132(22):42016.
- Kandola BK. Composites. In: *Fire Retardant Materials* Horrocks AR, Price D, eds. Boca Raton: CRC Press; 2001.
- Chae DW, Kim BC. Thermal and rheological properties of highly concentrated PET composites with ferrite nanoparticles. *Composites Science and Technology*. 2007;67(7-8):1348-1352.
- Fu S, Wu P, Han Z. Tensile strength and rupture energy of hybrid poly(methylvinylsiloxane) composites reinforced with short PET fibers and wollastonite whiskers. *Composites Science and Technology*. 2002;62(1):3-8.
- Scaffaro R, Botta L, Ceraulo M, La Mantia FP. Effect of kind and content of organo-modified clay on properties of PET nanocomposites. *Journal of Applied Polymer Science*. 2011;122(1):384-392.
- Hardjito D, Rangan BV. *Development and Properties of Low Calcium Fly ash based Geopolymer Concrete*. Curtin Research Report GC1. Perth: Curtin University of Technology; 2005.
- Catauro M, Papale F, Lamanna G, Bollino F. Geopolymer/PEG Hybrid Materials Synthesis and Investigation of the Polymer Influence on Microstructure and Mechanical Behavior. *Materials Research*. 2015;18(4):698-705.
- Nazari A, Khalaj G. Prediction total specific pore volume of geopolymers produced from waste ashes by fuzzy logic. *Materials Research*. 2012;15(2):242-252.
- Komnitsas K, Zaharaki D. Geopolymerisation: A review and prospects for the minerals industry. *Minerals Engineering*. 2007;20(14):1261-1277.
- Wu HC. Ductile ceramic-like materials by inorganic polymerization. *Materials Letters*. 2015;138:74-77.
- Ramos FJHTV, Mendes LC, Cestari SP. Organically modified concrete waste with oleic acid. *Journal of Thermal Analysis and Calorimetry*. 2015;119(3):1895-1904.
- Mendes LC, Silva DF, Lino AS. Linear low-density polyethylene and zirconium phosphate nanocomposites: evidence from thermal, thermo-mechanical, morphological and low-field nuclear magnetic resonance techniques. *Journal of Nanoscience and Nanotechnology*. 2012;12(12):8867-8873.
- ASTM International. *ASTM D 695-02 - Standard Test Method for Compressive Properties of Rigid Plastics*. West Conshohocken: ASTM International; 2002.
- Duxson P, Fernández-Jiménez A, Provis JL, Luckey GC, Palomo A, van Deventer JSJ. Geopolymer technology: the current state of the art. *Journal of Materials Science*. 2007;42(9):2917-2933.
- Singh B, Ishwarya G, Gupta M, Bhattacharya SK. Geopolymer concrete: A review of some recent developments. *Construction and Building Materials*. 2015;85:78-90.
- Chindapasirt P, Chalee W. Effect of sodium hydroxide concentration on chloride penetration and steel corrosion of fly ash-based geopolymer concrete under marine site. *Construction and Building Materials*. 2014; 63: 309-310.
- Edge M, Wiles R, Allen NS, McDonald WA, Mottock SV. Characterization of the species responsible for yellowing in melt degraded aromatic polyesters-I: Yellowing of poly(ethylene terephthalate). *Polymer Degradation and Stability*. 1996;53(2):141-151.

20. Silverstein RM, Webster FX. *Spectrometric Identification of Organic Compounds*. New York: Wiley; 1998.
21. Chen Z, Hay JN, Jenkins MJ. The thermal analysis of poly(ethylene terephthalate) by FTIR spectroscopy. *Thermochimica Acta*. 2013;552:123-130.
22. Piqué TM, Vázquez A. Uso de Espectroscopia Infrarroja con Transformada de Fourier (FTIR) en el estudio de la hidratación del cemento. *Concreto y cemento. Investigación y Desarrollo*. 2012;3(2):62-71.
23. Florea MVA, Brouwers HJH. Properties of various size fractions of crushed concrete related to process conditions and re-use. *Cement and Concrete Research*. 2013;52:11-21.
24. Barbhuiya SA, Gbagbo JK, Russell MI, Basheer PAM. Properties of fly ash concrete modified with hydrated lime and silica fume. *Construction and Building Materials*. 2009;23(10):3233-3239.
25. Prestsch E, Bühlmann P, Affolter C. *Structure Determination of Organic Compounds: Tables of Spectral Data*. Berlin, Heidelberg: Springer-Verlag; 2000.
26. Samperi F, Puglisi C, Alicata R, Montaudo G. Thermal degradation of poly (ethylene terephthalate) at the processing temperature. *Polymer Degradation and Stability*. 2004;83(1):3-10.
27. Ariffin MAM, Bhutta MAR, Hussin MW, Tahir MM, Aziah N. Sulfuric acid resistance of blended ash geopolymer concrete. *Construction and Building Materials*. 2013;43:80-86.
28. Greco A, Maffezzoli A, Manni O. Development of polymeric foams from recycled polyethylene and recycled gypsum. *Polymer Degradation and Stability*. 2005;90(2):256-263.
29. Chollet M, Horgnies M. Analyses of the surfaces of concrete by Raman and FT-IR spectroscopies: comparative study of hardened samples after demoulding and after organic post-treatment. *Surface and Interface Analysis*. 2011;43(3):714-725.
30. Allahverdi A, Najafi Kani E. Construction Wastes as Raw Materials for Geopolymer Binders. *International Journal of Civil Engineering*. 2009;7(3):154-160.
31. Ren X. *Complete Recycling and Utilization of Waste Concrete Through Geopolymerization*. [Dissertation]. Tucson: Department of Civil Engineering And Engineering Mechanics, The University of Arizona; 2015. 203 f.
32. Springfield T. *Application of FTIR for Quantification of Alkali in Cement*. [Thesis]. Denton: University of North Texas; 2011. 58 f.
33. Tantawy MA, Shatat MR, El-Roudi AM, Taher MA, Abd-El-Ramed M. Low Temperature Synthesis of Belite Cement Based on Silica Fume and Lime. *International Scholarly Research Notices*. 2014;2014:873215.
34. Yang K, Peng H, Wen Y, Li N. Re-examination of characteristic FTIR spectrum of secondary layer in bilayer oleic acid-coated Fe₃O₄ nanoparticles. *Applied Surface Science*. 2010;256(10):3093-3097.